Detergent-induced self-assembly and controllable photosensitizer activity of diester phenylene ethynylenes

Patrick L. Donabedian[a,b], Matthew N. Creyer[c], Florencia A. Monge[b,d], Kirk S. Schanze[e,1], Eva Y. Chi[b,f], and David G. Whitten[b,f,2]

[a]Nanoscience and Microsystems Engineering Graduate Program, University of New Mexico, Albuquerque, NM 87131; [b]Center for Biomedical Engineering, University of New Mexico, Albuquerque, NM 87131; [c]Department of Chemistry, University of Wisconsin–Madison, Madison, WI 53706; [d]Biomedical Engineering Graduate Program, University of New Mexico, Albuquerque, NM 87131; [e]Department of Chemistry, University of Florida, Gainesville, FL 32611; and [f]Department of Chemical and Biological Engineering, University of New Mexico, Albuquerque, NM 87131

Edited by Vivian Wing-Wah Yam, The University of Hong Kong, Hong Kong, China, and approved May 25, 2017 (received for review February 14, 2017)

Photodynamic therapy, in which malignant tissue is killed by targeted light exposure following administration of a photosensitizer, can be a valuable treatment modality but currently relies on passive transport and local irradiation to avoid off-target oxidation. We present a system of excited-state control for truly local delivery of singlet oxygen. An anionic phenylene ethynylene oligomer is initially quenched by water, producing minimal fluorescence and no measurable singlet oxygen generation. When presented with a binding partner, in this case an oppositely charged surfactant, changes in solvent microenvironment result in fluorescence unquenching, restoration of intersystem crossing to the triplet state, and singlet oxygen generation, as assayed by transient absorption spectroscopy and chemical trapping. This solvation-controlled photosensitizer model has possible applications as a theranostic agent for, for example, amyloid diseases.

photosensitizer | self-assembly | conjugated oligomers | photodynamic therapy | excited states

Generation of reactive oxygen species as a product of photoexcited electronic states in organic molecules can be a useful tool in a variety of applications. The possibilities of spatially localized generation of reactive oxygen species (ROS) in response to irradiation are only just beginning to be explored, despite the more than 100-y history of phototherapy in modern medicine (1), and are already in the clinic in the form of photodynamic therapy (PDT) for cancers of the skin, esophagus, and organ linings, actinic keratosis, and acne (2, 3). Photodynamic destruction of pathogenic bacteria, viruses, and fungi is also under investigation for antibiowarfare applications, passive sanitization of hospital surfaces under room light, and active sanitization of medical devices such as catheters (4–8). A major drawback of systemically dosed PDT photosensitizers, which are primarily porphyrins or their prodrugs (9), is their accumulation in the skin and eyes leading to long-lasting (weeks to months) posttherapeutic photosensitivity (10). Generation of ROS outside the target area can have multiple deleterious effects by overwhelming endogenous ROS-dependent signaling cascades (11). A solution to these issues would be a localized photosensitizer whose ROS-generating properties can be controllably activated, for example, in response to the binding to a target.

The motivation of the current study is to develop a tool for local delivery of singlet oxygen using binding and self-assembly–mediated control of excited states. Under intra- or intercellular conditions, 99% of singlet oxygen cannot travel more than 300 nm from the site of its generation before it decays through the transfer of its electronic energy to vibrational modes of water (12); the presence of redox sites will reduce this effective distance further. This less than 300-nm radius, being less than a cellular length, indicates that an active photosensitizer in or at a target cell will have minimal effect on adjacent cells. Previous investigations of switchable photosensitizers by various groups have used a pH-activatable rubyrin derivative (13), a quencher-tethered Si(IV) phthalocyanine (14) and pyropheophorbide (15), and various boron-dipyrromethene (BODIPY) dye-based scaffolds (16–18). Solvent microenvironment has been used to selectively photooxidize protein (19) and cellular targets (17), but only using intramolecular FRET quenching or solvent polarity effects on photoelectron transfer in BODIPY monomers or covalently linked dimers.

Control of photoexcited-state populations in organic molecules by the presence of quenchers is a common strategy in engineering sensor systems (Fig. 1). In the system at hand, the quencher is the network of solvating interfacial water molecules at the chromophoric esters of a p-phenylene ethynylene (OPE1 in Fig. 1), and the tool for controlling the presence of the quencher is complexation of the dye with low concentrations of an oppositely charged surfactant. Previous reports discovered that the presence of ethyl ester substituents on a phenylene ethynylene chromophore (Fig. 2) causes fluorescence to become highly quenched in water, presumably by quenching of the excited singlet state by a H-bonding or partial proton-transfer mechanism (20–22). These dyes with low fluorescence in polar aqueous environments and high fluorescence in nonpolar environments are useful sensors for amyloid protein aggregates, to which they bind with moderate affinity (23). Furthermore, the presence of oppositely charged surfactants (24), lipids (25), or other scaffolds (21) can induce these dyes to form J-type

Significance

Photosensitizers harvest light energy and transfer it to ground-state molecular oxygen, producing singlet oxygen, a powerful oxidizer. This property can be exploited for targeted removal of diseased or cancerous tissue, but most currently available photosensitizers do not display any molecular specificity. We discovered that diester phenylene ethynylenes exhibit switchable photosensitizer activity based on their immediate molecular environment, and used detergent-induced self-assembly to demonstrate that these molecules present an attractively compact switchable photosensitizer system.

Author contributions: P.L.D., M.N.C., F.A.M., K.S.S., E.Y.C., and D.G.W. designed research; P.L.D., M.N.C., and F.A.M. performed research; P.L.D., M.N.C., F.A.M., E.Y.C., and D.G.W. analyzed data; and P.L.D., E.Y.C., and D.G.W. wrote the paper.

The authors declare no conflict of interest.

This article is a PNAS Direct Submission.

[1]Present Address: Department of Chemistry, University of Texas at San Antonio, San Antonio, TX 78249.

[2]To whom correspondence should be addressed. Email: whitten@unm.edu.

This article contains supporting information online at www.pnas.org/lookup/suppl/doi:10.1073/pnas.1702513114/-/DCSupplemental.

www.pnas.org/cgi/doi/10.1073/pnas.1702513114

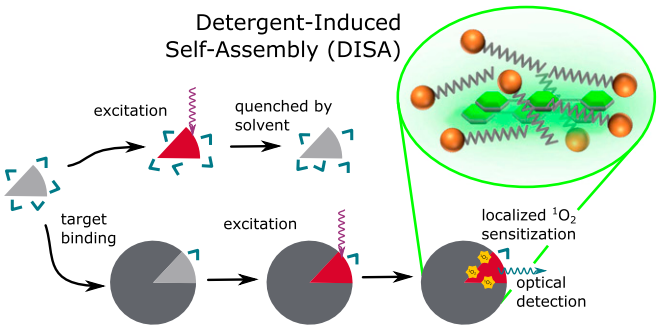

Fig. 1. Schematic of DISA model of targeted singlet oxygen sensitization and optical detection.

aggregates with enhanced emission and usefully placed electronic transitions (i.e., in the visible rather than UV range) (26). Because the excited singlet state is upstream of triplet states and photosensitizer activity, as well as fluorescence (Fig. 3), we hypothesized that ester-functionalized oligo-p-phenylene ethynylene (OPEs) would not have significant photosensitizer activity when solubilized in water, but would gain both long-lived excited triplet states and ROS generation when complexed with an oppositely charged surfactant displacing the solvent. In this study, surfactant binding-activated unquenching of an anionic OPE, OPE1 (Fig. 2) was characterized. Concomitant changes in the OPE's excited-triplet-state lifetime and ROS generation were tested using transient absorption spectroscopy and chemical trapping, respectively.

Results and Discussion

Detergent-Induced Self-Assembly and Unquenching of OPE Fluorescence. Addition of the cationic surfactant cationic surfactant cetyl trimethylammonium bromide (CTAB) to a solution of anionic OPE1 in water resulted in dramatic changes to both the absorbance and fluorescence emission spectra of OPE1 (Fig. 4). Addition of CTAB caused significant increases in OPE1 fluorescence yield without significant distortion of peak placement in the emission spectra (Fig. 4*B*). Similar unquenching was seen with amyloid protein fibrils (23) as well as carboxylated starches (21) for a variety of ester-terminated OPEs with varying lengths. The enhancement of excited-singlet-state populations in the presence of detergent opens the possibility of enhanced triplet production and promotion of singlet oxygen generation (Fig. 4). Under the quenched conditions, no triplet states are available to sensitize singlet oxygen, but when solvent is displaced by binding to a hydrophobic target, the fluorescence is restored along with the potential for singlet oxygen generation.

The absorbance spectra of the OPE exhibit a redshift together with onset of fluorescence and are similar to those previously reported for a cationic OPE with an anionic detergent under similar submicellar conditions (24). The quantum yield of fluorescence of the cationic analogue of OPE1 (di-quaternary ammonium salt) is 0.023 in water and 0.75 in methanol (20). Brightness of fluorescence has been observed to be identical between this compound and OPE1. Upon addition of stoichiometric surfactant with the appropriate charge, either compound regains fluorescence as bright as that in methanol. From these observations and results, we postulate that the fluorescence quantum yield of surfactant-bound OPE1 is at or near 0.75. The other 25% of excited states mostly contributes to the generation of singlet oxygen. For both OPE1 and other OPEs with "ionic side arms," this effect has been attributed to the formation of a complex including an OPE dimer and several detergent molecules. This detergent-induced self-assembly (DISA) is interesting in that there is no association between or aggregation of either reagent in water at these concentrations; the ion-pairing and local concentration effect of the surfactant is necessary to allow the OPEs to approach one another and dimerize. The addition of 3 μM CTAB, a 3:2 ratio of detergent to OPE1, induces a spectral shift indicating significant conversion of the OPE1 to a J dimer (Fig. 4*A*). Dynamic light-scattering results (*SI Appendix*, Fig. S8) indicate that CTAB micelles with and without OPE1 both have hydrodynamic radii of roughly 35 nm, with premicellar aggregates too small to reliably measure. As shown below, as well as activating fluorescence, DISA can induce a photochemical reaction that is not possible without detergent by extending the lifetime of the excited singlet state.

DISA-Controlled Generation of OPE1 Triplet Excited States. To gain direct information about the number of triplet excited states available to transfer energy to singlet oxygen, the intensity and lifetime of the triplet–triplet absorption were measured by transient absorption experiments (Figs. 5 and 6). Initially H_2O solutions of OPE1 had no detectable transient absorption after 35-ns delay (Fig. 5, *Top*), consistent with near-complete quenching

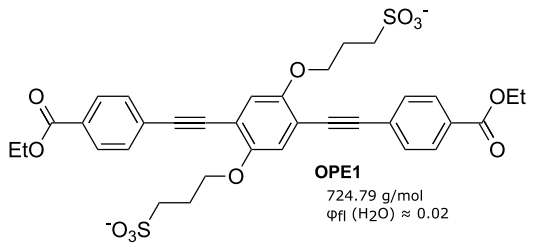

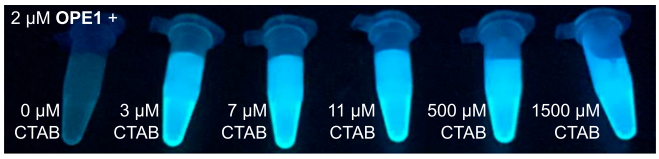

Fig. 2. Structure of anionic OPE1 (*Top*) and pictures of 2 μM OPE1 in water or water containing varying concentrations of cationic detergent CTAB under UVA illumination.

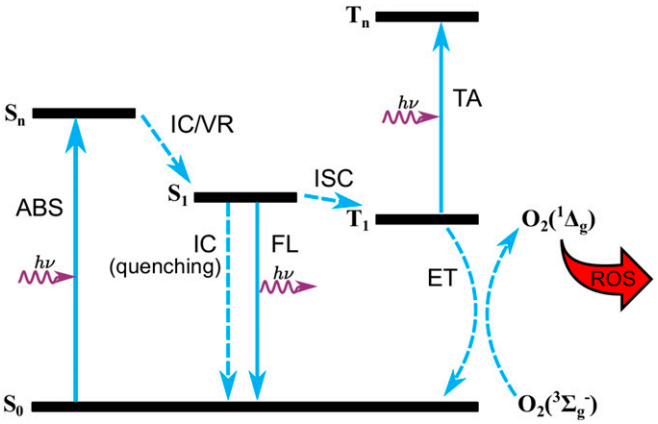

Fig. 3. Simplified Jablonski diagram of OPE1 electronic states. After excitation by photon absorption (ABS) and fast internal conversion and vibrational relaxation (IC/VR) to the S_1 state, three competing decay processes exist: first, nonradiative, solvent-mediated quenching by internal conversion (IC), second, radiative decay by fluorescence (FL), and third, crossing to the triplet manifold by intersystem conversion (ISC) and subsequent energy transfer (ET) to produce singlet oxygen ($^1O_2$) from ground-state dioxygen. The relative rates of these three processes determine the functional behavior of the system. Triplet states can be assayed by the triplet–triplet TA process.

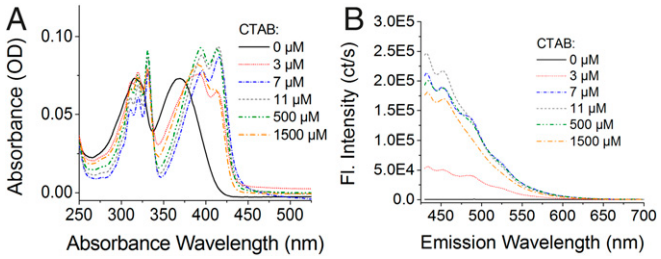

Fig. 4. Absorbance (*A*) and fluorescence emission (*B*) spectra of samples containing 2.0 μM OPE1 and varying CTAB concentrations using λ_{ex} = 420 nm.

of the excited singlet state before intersystem crossing can occur (Fig. 3). Titration of CTAB in 1-μM increments caused a transient absorbance peak centered at 600 nm to appear, which became strong enough to measure its lifetime at 4 μM CTAB. The intensity of the transient absorption saturated at about 10 μM CTAB (Fig. 6*B*), indicating that all OPE1 was complexed at this concentration. Lifetime values (τ) of the triplet–triplet transient absorption (TA in Fig. 3) were fairly constant at low CTAB concentrations (3–10 μM), averaging around 25 μs, and decreased gradually at a higher CTAB concentration (8 μs for 49 μM) (Fig. 6*B*). This decrease in τ could be an artifact of residual oxygen present, as foam formation in the higher-concentration CTAB solutions prohibited the complete removal of oxygen from the samples, or it could be the result of triplet–triplet annihilation due to the complexing action of the surfactant bringing multiple excited states into close proximity. The former explanation seems more likely because, as noted below, generation of ROS by OPE1 continues to increase with increasing CTAB concentration into the millimolar regime (*SI Appendix*, Fig. S2).

Interestingly, the OPE1 triplet–triplet absorption is significantly different in shape and wavelength from that of the related dye without ester substituents (*SI Appendix*, Fig. S4), indicating that either the esters have an impact on the electronic structure and the T_1–T_n transition or the triplet state is delocalized across a J dimer. The effect of changing ground-state absorption over the CTAB concentration range complicates the interpretation of the spectra, but the lack of isosbestic points indicates that multiple singlet states may be involved, supporting the presence of a monomer–J-dimer equilibrium in the OPE molecules.

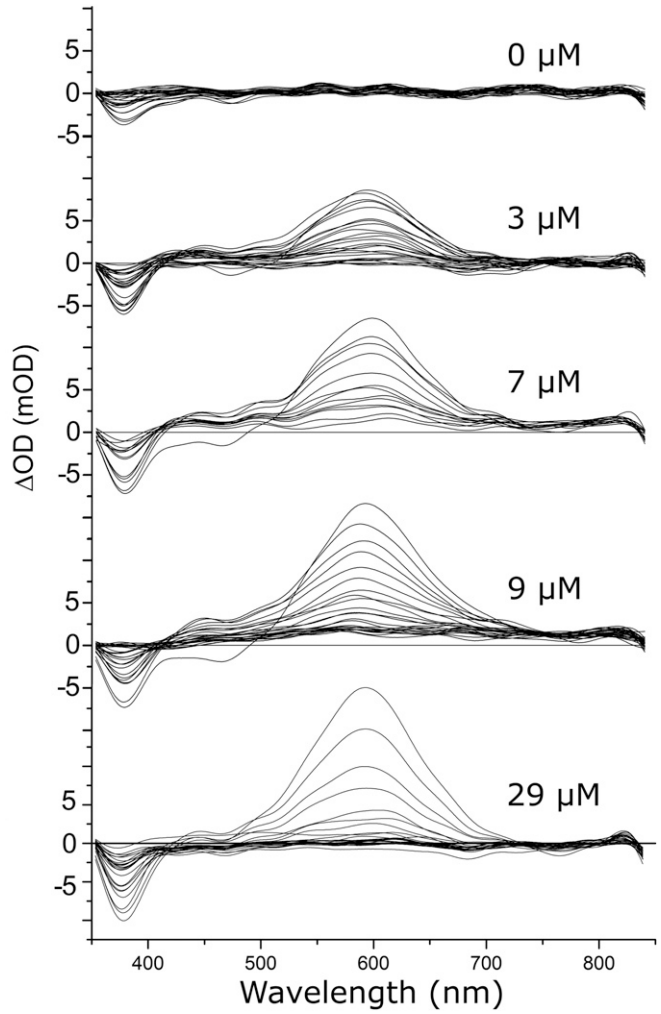

Fig. 5. TA difference spectra of OPE1 (2 μM) in water with differing CTAB concentrations. Initial delay was 35 ns and delay time increased in 3-μs increments until TA returned to baseline. Oxygen was largely removed by bubbling with argon gas.

Solvent-Controlled ROS Generation Assayed by Chemical Trapping. To measure the chemical activity of the singlet oxygen produced by OPE1 as a result of DISA, chemical-trapping experiments were carried out to detect the generation of ROS by OPE1. The effect of OPE1 complexation with various concentrations of CTAB, below and above CTAB critical micelle concentration (CMC), on singlet oxygen sensitization was assayed using 9,10-anthracenediyl-bis(methylene)dimalonic acid (ADMA, *SI Appendix*, Fig. S3) as a chemical sensor (27). The ADMA is bleached in the near-UV by cycloaddition of oxygen across the central ring of the anthracene chromophore, leading to a reduction in the absorbance band at 261 nm (27).

Fig. 7 shows the absorption spectra of solutions of ADMA (1.5 μM), OPE1 (2 μM), and varying below CMC concentrations of CTAB (0, 3, 7, and 11 μM) before (Fig. 7*A*) and after (Fig. 7*B*) 3.5 min of 420-nm centered broadband light irradiation. Absorption spectra of control samples containing the same concentrations of ADMA and CTAB, but not OPE1, before (Fig. 7*C*) and after (Fig. 7*D*) irradiation are also plotted. These absorbance measurements were not converted to quantum-yield values due to the strong local concentration effects of the surfactant; the changes in absorbance are taken as a semiquantitative measure of singlet oxygen generation. The strong band at 261 nm arises from ADMA and the lower energy transitions (above 300 nm) arise primarily from OPE1, with a small contribution from the anthracene (Fig. 7*C*). When mixed with CTAB and ADMA, the OPE1 bands in Fig. 8*A* show significant redshifts compared with OPE1 bands without CTAB (Fig. 7*A*). The appearance of OPE1 vibronic structure is consistent with the formation of surfactant-mediated J-type dimers (24) complexed

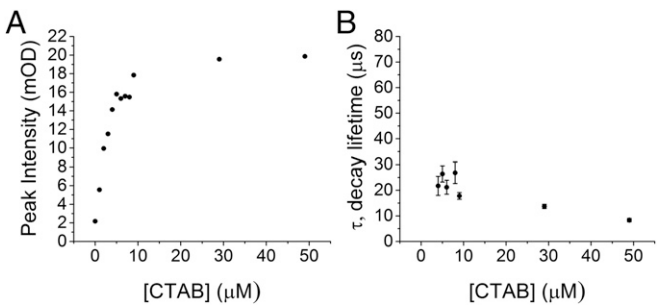

Fig. 6. Intensity (ΔOD) (*A*) and triplet lifetime (*B*) of triplet–triplet absorption in OPE1 (2 μM) solutions containing varying concentrations of CTAB.

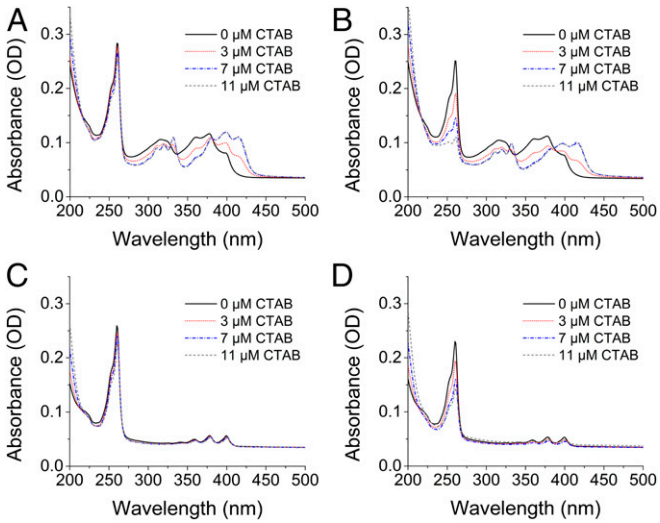

Fig. 7. Absorbance spectra of samples containing 2 μM OPE1, 1.5 μM ADMA, and 0–11 μM CTAB before (*A*) and after (*B*) 420-nm centered light irradiation and controls containing 1.5 μM ADMA and 0–11 μM CTAB, but no OPE1, before (*C*) and after (*D*) irradiation. CTAB-induced bleaching above background was observed in the ADMA peak at 261 nm, concomitant with redshifting and appearance of vibronic structure in OPE1 bands at 320 and 364 nm.

with detergent molecules. With irradiation at 420-nm light which is predominantly absorbed by the OPE1 (Fig. 4*A*), the ADMA peak at 261 nm shows CTAB-induced bleaching, indicating the onset of photosensitizer activity of OPE1 in the detergent-complexed state. The loss of absorbance at 261 nm results from singlet-oxygen-specific cycloaddition across the central ring of ADMA (27). Controls of light irradiation of ADMA alone (Fig. 7 *C* and *D*) indicate that the anthracene exhibits some CTAB-concentration-dependent self-bleaching, consistent with more persistent excited states arising from reduced local solvent polarity (28). These results indicate that CTAB, an oppositely charged detergent, mediates self-assembly of OPE1 monomers into J-type dimers with long-lived excited states and both bright fluorescent emission and relatively efficient photosensitizer activity (22).

With an eye toward a future application in cellular delivery, we also tested the robustness of OPE1 photosensitization by testing the compound at higher concentrations of CTAB, near and above micellar concentrations. Fig. 8 shows the absorbance spectra before and after irradiation of ADMA (21.4 μM) and OPE (21.4 μM) samples containing 0.5 mM (below CMC) and 1.5 mM (above CMC) CTAB. Concentrations of ADMA and OPE were raised in these samples to match the molar concentrations of CTAB micelles at 1.5 mM, using an aggregation

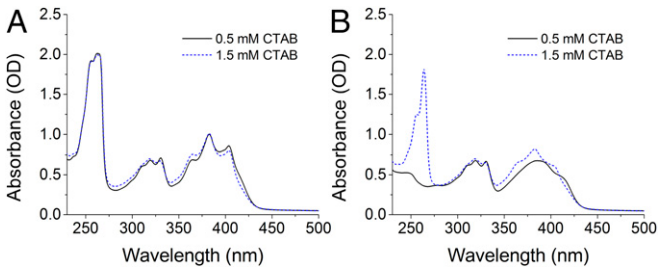

Fig. 8. Absorbance spectra of samples containing 21.4 μM OPE1, 21.4 μM ADMA, and 0.5 mM or 1.5 mM CTAB before (*A*) and after (*B*) 420-nm centered light irradiation.

number of 70 for CTAB (28). Fig. 8 shows the absorbance spectra of the samples before (Fig. 8*A*) and after (Fig. 8*B*) light irradiation. Note that the absorbance of the ADMA peak of these high-ADMA-concentration samples were saturated at OD ~2.0 (Fig. 8*A*). Using Beer's law, the absorbance of ADMA at 21.4 μM is expected to be ~4.8. After light irradiation, absorbance value of ADMA peak in samples containing 0.5 and 1.5 mM CTAB significantly decreased to about 0.5 and 1.75, respectively (Fig. 8*B*), corresponding to ~90% and 65% bleaching. Control samples that contained ADMA and CTAB, but not OPE, were also prepared and measured. As we had previously observed, self-bleaching of ADMA also occurred in these high-CTAB-concentration controls. However, because OPE was the dominant absorbing species in the samples at 420 nm, it is reasonable to conclude that ADMA bleaching in samples containing OPE1 was primarily through photosensitization of OPE1. Although the effect of ADMA self-bleaching cannot be quantitatively accounted for, these results confirm that DISA-activated OPE1 photosensitizer activity is retained at high detergent concentrations.

The proposed physical model for the response of OPE1 dyes to increasing surfactant concentration is summarized in Fig. 9. In the absence of surfactant, OPE1 molecules are dissolved as monomers in solution, and their singlet excited states are efficiently quenched by solvent interaction resulting in low fluorescence and near-zero intersystem crossing. In the submicellar CTAB regime, OPE1–detergent interactions shield OPE1 from water quenching, and lead to OPE1 J-type dimer formation and redshifting of the absorption bands. Similar effects are seen in the micellar regime even as the equilibrium shifts back from J dimers to monomers. As a result, detergent-complexed OPE1 exhibits increased fluorescence and availability of singlet states for intersystem crossing.

Conclusions

The results of this study establish a bis(ethyl ester)phenylene ethynylene as a switchable photosensitizer system, with DISA that causes the displacement of solvating waters by the binding to a more hydrophobic target. Low concentrations of oppositely charged detergent restored powerful photosensitizer activity to OPE1 while also generating a J band in absorbance and increasing fluorescence emission 100-fold. DISA-mediated effects begin to take hold with stoichiometric amounts of detergent, become strongest around a 5:1 CTAB:OPE1 ratio, and continue to be effective well into micellar regimes. These results indicate that this or related molecules could be used to selectively photooxidize any hydrophobic binding partner capable of desolvating the ethyl ester quencher groups. The micromolar affinity of the OPE1 compound for amyloid fibrils represents an inviting

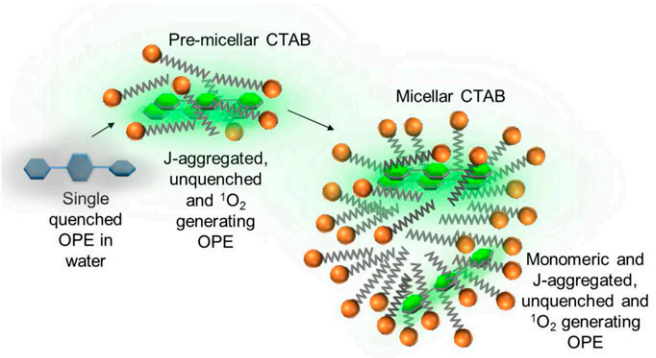

Fig. 9. Schematic of DISA of OPE1 and associated changes in the photophysical properties of OPE1.

direction beyond oncology for singlet oxygen delivery, although the problem of delivering excitation energy to target organs remains unsolved. Similar phenylene ethynylenes are also seen to interact with various starch-based substrates (8, 21), making pathogenic fungi a possible target as well.

Compared with previous efforts in the same field, the OPE-based system is attractively compact, requiring no external quencher or specificity-granting conjugate. The quenching-granting groups add little steric bulk, and the chromophore's own binding profile can provide specificity for several useful substrates. One downside of this approach is that reengineering the binding profile to hit different targets or optimize binding without altering key photophysical properties may be challenging. We are confident that continued efforts to improve understanding and flexibility of this system will be successful. Overall these results present ester-functionalized phenylene ethynylenes as an environment-switchable photosensitizer with a mechanism for site-specific photodynamic therapy.

Materials and Methods

General. Synthesis and purification of OPEs including OPE1 has been described previously (21). ADMA and CTAB were obtained from Sigma-Aldrich Chemical Co. and used without further purification. Water used in all experiments was purified to a resistivity of 18.2 MΩ by a Synergy Millipore UV filtration system (EMD Millipore). Sizes of premicellar and micellar CTAB and CTAB-OPE complexes were measured with dynamic light scattering on a DAWN HELEOS-II light-scattering detector (Wyatt Technologies).

TA Spectroscopy. Triplet–triplet TA spectra were obtained using a pump–probe technique with the third harmonic of a Nd:YAG laser (Continuum Surelite) as the pump illumination source and a Xe flash lamp as the probe illumination source. Two transmission spectra (one from a region of the sample illuminated by the pump beam) were obtained by passing the probe light through a blaze grating onto a gated-intensified CCD camera, and their difference was used to calculate the final TA difference spectra. The instrument was controlled using LabVIEW and postprocessing performed using MATLAB. A fast Fourier transform filter with a 20-nm window was applied to spectra to reduce high-frequency noise and improve readability; the original data can be found in *SI Appendix*, Fig. S1. The setup, including details of calibration, optical diagrams, hardware, and timing electronics, has been described elsewhere (29).

Solutions of OPEs (2 μM) were prepared at 0.8-OD absorbance at 355 nm in a 10-mL, 1-cm-pathlength recirculating cuvette with magnetic stirrer. Samples were excited at 355 nm with a constant pulse fluence of ∼20 mJ cm^{-2}. The cuvette was sealed with a rubber septum and the sample was sparged with argon for 30 min before each experiment. Initial delay was set at 35 ns to allow time for triplet crossing. Delay time increased in 3-μs increments between spectra until TA returned to baseline. A stock CTAB solution was added to the OPE sample incrementally by syringe and the solution was sparged between readings.

$^1O_2$ Detection by Chemical Trapping. OPE1 concentration was determined by UV/visible spectrophotometry (PerkinElmer Lambda 35 UV/Visible Spectrophotometer) using an extinction coefficient of 3.92×10^4 L $mol^{-1} \cdot cm^{-1}$, identical to the cationic analog (21). All spectroscopy was performed in 1-cm-pathlength fused-quartz cuvette with 0.55 mL of solution. Samples containing varying concentrations of OPE1, ADMA, and CTAB were exposed to light irradiation in quartz cuvettes on a rotating carousel in a photochamber using eight LZC 420 lamps (Luzchem Research Inc.), with emission centered at 420 nm and total incident power of 2.28 ± 0.028 mW cm^{-2} (7). Low CTAB concentration samples (2 μM OPE1, 1.5 μM ADMA, and 0–11 μM CTAB) were irradiated for 5 min, and higher-CTAB-concentration samples (0.5- and 1.5 mM CTAB) were irradiated for 3.5 min. For the 1.5 mM CTAB (above CTAB CMC) samples, solutions were prepared with low (2 μM OPE1, 1.5 μM ADMA) and equal molar concentrations (21.4 μM) of OPE1, ADMA, and CTAB micelles. Using an aggregation number of 70 for CTAB (28), 21.4 μM was calculated as the concentration of micelles in a 1.5 mM CTAB solution Fluorescence samples for the determination of OPE unquenching and aggregation were performed in quartz cuvettes using a PTI QuantaMaster 40 fluorometer.

ACKNOWLEDGMENTS. Austin Jones and Dave Bullock provided vital technical support for TA instrumentation, and Dr. Yanli Tang and Dr. Eunkyung Ji originally synthesized the OPEs. We gratefully acknowledge the National Science Foundation (NSF) for Awards NSF 1207362 and NSF 1605225 awarded to E.Y.C. and NSF 1263387 in support of M.N.C., as well as Defense Threat Reduction Agency Grant HDTRA1-08-1-0053.

1. Dolmans DE, Fukumura D, Jain RK (2003) Photodynamic therapy for cancer. *Nat Rev Cancer* 3:380–387.
2. Cui X, Zhao J, Zhou Y, Ma J, Zhao Y (2014) Reversible photoswitching of triplet-triplet annihilation upconversion using dithienylethene photochromic switches. *J Am Chem Soc* 136:9256–9259.
3. Ericson MB, Wennberg A-M, Larkö O (2008) Review of photodynamic therapy in actinic keratosis and basal cell carcinoma. *Ther Clin Risk Manag* 4:1–9.
4. Johnson GA, Muthukrishnan N, Pellois JP (2013) Photoinactivation of Gram positive and Gram negative bacteria with the antimicrobial peptide (KLAKLAK)(2) conjugated to the hydrophilic photosensitizer eosin Y. *Bioconjug Chem* 24:114–123.
5. Li K, et al. (2014) Selective photodynamic inactivation of bacterial cells over mammalian cells by new triarylmethanes. *Langmuir* 30:14573–14580.
6. Baptista MS, Wainwright M (2011) Photodynamic antimicrobial chemotherapy (PACT) for the treatment of malaria, leishmaniasis and trypanosomiasis. *Braz J Med Biol Res* 44:1–10.
7. Parthasarathy A, et al. (2015) Conjugated polyelectrolytes with imidazolium solubilizing groups. Properties and application to photodynamic inactivation of bacteria. *ACS Appl Mater Interfaces* 7:28027–28034.
8. Pappas HC, et al. (2016) Antifungal properties of cationic phenylene ethynylenes and their impact on β-glucan exposure. *Antimicrob Agents Chemother* 60:4519–4529.
9. Allison RR, et al. (2004) Photosensitizers in clinical PDT. *Photodiagn Photodyn Ther* 1: 27–42.
10. Moriwaki SI, et al. (2001) Analysis of photosensitivity in Japanese cancer-bearing patients receiving photodynamic therapy with porfimer sodium (Photofrin). *Photodermatol Photoimmunol Photomed* 17:241–243.
11. Brieger K, Schiavone S, Miller FJ, Jr, Krause K-H (2012) Reactive oxygen species: From health to disease. *Swiss Med Wkly* 142:w13659.
12. Redmond RW, Kochevar IE (2006) Spatially resolved cellular responses to singlet oxygen. *Photochem Photobiol* 82:1178–1186.
13. Tian J, et al. (2013) Cell-specific and pH-activatable rubyrin-loaded nanoparticles for highly selective near-infrared photodynamic therapy against cancer. *J Am Chem Soc* 135:18850–18858.
14. Lau JTF, Lo PC, Jiang XJ, Wang Q, Ng DKP (2014) A dual activatable photosensitizer toward targeted photodynamic therapy. *J Med Chem* 57:4088–4097.
15. Zheng G, et al. (2007) Photodynamic molecular beacon as an activatable photosensitizer based on protease-controlled singlet oxygen quenching and activation. *Proc Natl Acad Sci USA* 104:8989–8994.
16. Zhang XF, Yang X (2013) Photosensitizer that selectively generates singlet oxygen in nonpolar environments: Photophysical mechanism and efficiency for a covalent BODIPY dimer. *J Phys Chem B* 117:9050–9055.
17. Kolemen S, et al. (2015) Intracellular modulation of excited-state dynamics in a chromophore dyad: Differential enhancement of photocytotoxicity targeting cancer cells. *Angew Chem Int Ed Engl* 54:5340–5344.
18. Jiang XD, et al. (2015) Synthesis of NIR naphthyl-containing aza-BODIPYs and measure of the singlet oxygen generation. *Tetrahedron* 71:7676–7680.
19. Yogo T, et al. (2008) Selective photoinactivation of protein function through environment-sensitive switching of singlet oxygen generation by photosensitizer. *Proc Natl Acad Sci USA* 105:28–32.
20. Tang Y, et al. (2009) Photophysics and self-assembly of symmetrical and unsymmetrical cationic oligophenylene ethynylenes. *J Photochem Photobiol Chem* 207: 4–6.
21. Tang Y, et al. (2011) Synthesis, self-assembly, and photophysical properties of cationic oligo(p-phenyleneethynylene)s. *Langmuir* 27:4945–4955.
22. Hill EH, Evans DG, Whitten DG (2014) The influence of structured interfacial water on the photoluminescence of carboxyester-terminated oligo-p-phenylene ethynylenes. *J Phys Org Chem* 27:252–257.
23. Donabedian PL, Pham TK, Whitten DG, Chi EY (2015) Oligo(p-phenylene ethynylene) electrolytes: A novel molecular scaffold for optical tracking of amyloids. *ACS Chem Neurosci* 6:1526–1535.
24. Hill EH, Sanchez D, Evans DG, Whitten DG (2013) Structural basis for aggregation mode of oligo-p-phenylene ethynylenes with ionic surfactants. *Langmuir* 29: 15732–15737.
25. Hill EH, Zhang Y, Evans DG, Whitten DG (2015) Enzyme-specific sensors via aggregation of charged *p*-phenylene ethynylenes. *ACS Appl Mater Interfaces* 7:5550–5560.
26. Würthner F, Kaiser TE, Saha-Möller CR (2011) J-aggregates: From serendipitous discovery to supramolecular engineering of functional dye materials. *Angew Chem Int Ed Engl* 50:3376–3410.
27. Kuznetsova NA, et al. (2001) New reagents for determination of the quantum efficiency of singlet oxygen generation in aqueous media. *Russ J Gen Chem* 71:36–41.
28. Bowen EJ, West K (1955) Solvent quenching of the fluorescence of anthracene. *J Chem Soc* 53:4394.
29. Farley RT (2007) Photophysics of platinum and iridium organometallic materials: From molecular wires to nonlinear optics. PhD dissertation (University of Florida, Gainesville).